International Journal of Thermophysics, Vol. 23, No. 6, November 2002 (© 2002)

An Absolute Viscometer-Densimeter and Measurements of the Viscosity of Nitrogen, Methane, Helium, Neon, Argon, and Krypton over a Wide Range of Density and Temperature

C. Evers,[1] H. W. Lösch,[1] and W. Wagner[1, 2]

Received January 7, 2002

An apparatus for the simultaneous measurement of viscosity and density of fluids is presented. The viscometer-densimeter covers a viscosity range up to 150 μPa·s and a density range up to 2000 kg·m^{-3} at temperatures from 233 to 523 K and pressures up to 30 MPa. Very accurate density measurements with uncertainties of ±0.02 to ±0.05% have always been carried out with this apparatus, although in its first version it was necessary to calibrate the viscosity measuring system on a reference fluid in order to achieve uncertainties of ±0.6 to ±1.0% in viscosity. After significant improvements, the apparatus now achieves uncertainties in viscosity of less than ±0.15% in the dilute gas region and less than ±0.4% for higher densities. Moreover, the viscosity measuring system can be described in an absolute way; calibration is no longer necessary. In order to test the advanced apparatus and to determine viscosity-density values of very high quality, comprehensive measurements on nitrogen, argon, and methane were carried out in the entire working range of the viscometer-densimeter. In addition, viscosity-density measurements on helium, neon, and krypton were made on two selected isotherms each. All measurements show that the estimated total uncertainty of ±0.15 to ±0.4% in viscosity and of ±0.02 to ±0.05% in density is clearly met. In order to verify the results of the combined viscometer-densimeter, a new apparatus for very accurate viscosity measurements was designed. While the working range of this apparatus is restricted to the dilute gas region, it yields uncertainties of less than ±0.07% in viscosity. Measurements carried out with this apparatus confirmed the previously measured values of the combined viscometer-densimeter within ±0.03%.

KEY WORDS: argon; density; helium; krypton; magnetic suspension coupling; methane; neon; nitrogen; simultaneous viscosity and density measurement; single-sinker densimeter; viscometer; viscosity.

[1] Lehrstuhl für Thermodynamik, Ruhr-Universität Bochum, D-44780 Bochum, Germany.
[2] To whom correspondence should be addressed. E-mail: Wagner@thermo.ruhr-uni-bochum.de

0195-928X/02/1100-1411/0 © 2002 Plenum Publishing Corporation

1. INTRODUCTION

There are two important reasons for simultaneously measuring viscosity and density. The first is that the best description of the viscosity behavior of fluids over wide ranges of temperature and pressure is gained with correlations depending on temperature and density. The second is that the density is needed to achieve the highest possible accuracies in viscosity measurement. The density is an essential part of the working equation used to determine the viscosity from the measuring signal, regardless of the type of the viscometer.

Ideally, one instrument to measure both the density together with the viscosity is needed. There are measuring principles (oscillating disk and oscillating wire) that generally meet this requirement, but their measuring range is limited to the liquid region; see, for example, [1–3]. Nevertheless, in most cases the viscosity was measured together with temperature and *pressure* instead of temperature and *density*. Instead of the direct measurement, the density of the investigated fluid was calculated from an equation of state. Obviously, this procedure limits accurate viscosity measurements and correlations to fluids for which sufficiently accurate equations of state exist. At present these are available only for about 25 pure substances. In the case of mixtures, only a few natural gases and refrigerant mixtures meet this requirement.

Consequently, in our group an apparatus for the simultaneous measurement of viscosity and density of fluids in one compact measuring cell was developed [4, 5]. The main element of the instrument is an electronically controlled magnetic suspension coupling [6]. To carry out the density measurement (buoyancy principle according to the single-sinker method [7, 8]), this coupling is used for the contactless transfer of the forces acting on a sinker in the measuring cell to a microbalance. Besides this, the coupling serves as a frictionless bearing for a slender cylindrical body. The rotation of this freely rotating cylinder is slowed due to the viscous drag of the fluid surrounding the cylinder. The viscosity of the fluid can be directly determined from the decay rate of the rotational frequency.

The viscometer-densimeter covers a large operational range with respect to pressure and temperature. It has always achieved excellent uncertainties in density measurement and also small uncertainties in viscosity measurement. Now, after additional development, the uncertainties in viscosity have been decreased even further and the viscosity measuring principle can be considered as an absolute measuring principle.

In this paper the modifications carried out on the viscometer-densimeter are described. Furthermore, viscosity-density measurements on nitrogen, methane, helium, neon, argon, and krypton carried out with the

advanced viscometer-densimeter are presented. Finally, a new, special apparatus for very accurate viscosity measurements at low densities was designed in order to verify the results of the viscometer-densimeter. The principle and the first experimental results of this special apparatus are also presented in this paper.

2. BASIC PRINCIPLE OF THE COMBINED VISCOMETER-DENSIMETER

A detailed description of the combined viscometer-densimeter can be found in Refs. 4 and 5. Figure 1 shows the principle of the first version of the viscometer-densimeter.

2.1. Density Measurement

The density is measured by the buoyancy principle according to the single-sinker method [7, 8]. A cylindrical sinker is placed within a closed

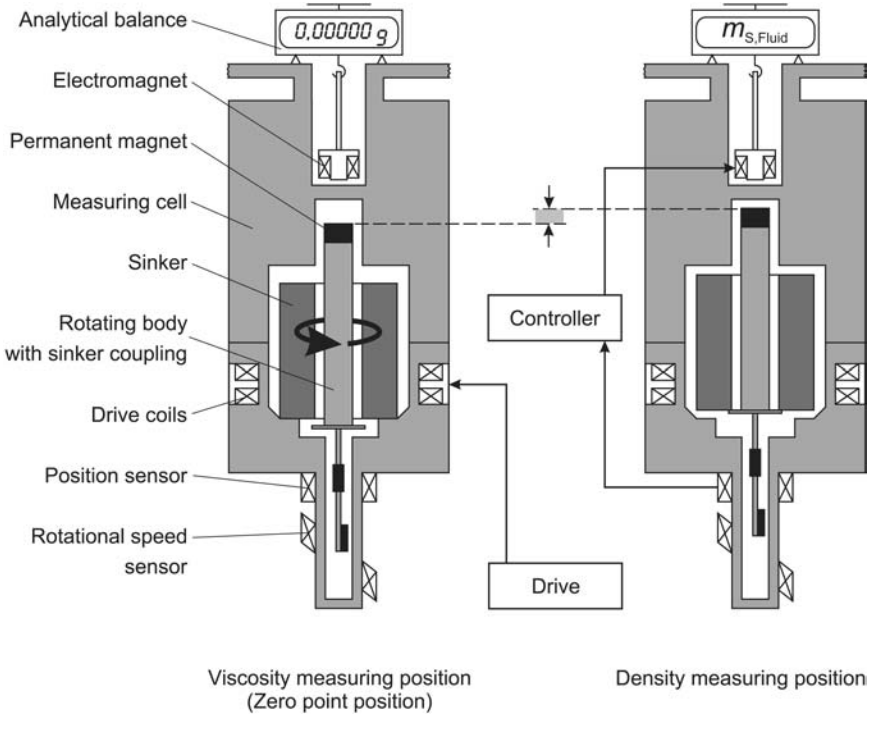

Fig. 1. Principle of the viscometer-densimeter.

measuring cell, which is filled with the fluid whose density should be measured. The buoyancy force exerted upon the sinker by the fluid is directly measured with a microbalance. The density of the fluid can be determined from the working equation of the densimeter:

$$\rho = \frac{m_S - m_{S,\,\mathrm{Fluid}}}{V_S(T, p)} = \frac{\Delta m_{\mathrm{buoyancy}}}{V_S(T, p)}. \tag{1}$$

In this equation, m_S is the "true" mass of the sinker (weighed in the evacuated measuring cell), $m_{S,\,\mathrm{Fluid}}$ is the "apparent" mass of the sinker (weighed in the fluid-filled measuring cell), and $V_S(T, p)$ is the temperature- and pressure-dependent volume of the sinker. The value of $V_S(T, p)$ is approximately 13 cm^3 and known from calibration with water at $T_0 = 293.15$ K and $p_0 = 0.1$ MPa with a calibration uncertainty $\leqslant \pm 0.003\%$. The dependence of the volume of the titanium sinker on temperature and pressure is known very accurately.

The essential feature of the single-sinker method is that the forces acting upon the sinker are transferred without contact through the wall of the pressurized measuring cell by an electronically controlled magnetic suspension coupling to the balance, which is placed at ambient conditions. The electromagnet is attached to the balance and carries the permanent magnet which is placed inside the measuring cell. Since this condition is physically not stable, the vertical position of the permanent magnet is controlled with an inductive sensor and an electronic control unit maintains a stable free suspension state of the permanent magnet.

In order to achieve the highest possible accuracies it is necessary to define and to control the zero point of the weighing. Therefore, the permanent magnet can be suspended in two different vertical positions. In the position shown on the left side of Fig. 1, only the permanent magnet and the rotating body for carrying the sinker are suspended. The sinker itself rests at the bottom of the measuring cell. In this position the zero point is recorded to correct the measuring result. The permanent magnet can be moved upward into a position which is about five millimeters higher than the zero point position. In this way the sinker is lifted up and coupled to the weighing system and the buoyancy force $\Delta m_{\mathrm{buoyancy}}$ [see Eq. (1)] exerted upon the sinker is directly measured. This is the density measuring position shown on the right side of Fig. 1.

2.2. Viscosity Measurement

The magnetic coupling not only allows the contactless transfer of forces, but it is also a frictionless bearing with regard to the rotation of the

permanent magnet around its vertical axis. This feature of the magnetic suspension coupling is the basis of the viscosity measuring principle.

During the viscosity measurement the rotating body with the permanent magnet remains in the zero-point position mentioned before (see Fig. 1). The freely suspended permanent magnet is embedded in the rotating body, which is immersed in the fluid. The rotating body has the shape of a slender cylinder, which is produced from an aluminum alloy with good electrical conductivity. It is surrounded concentrically by the sinker and the wall of the measuring cell. At the beginning of a viscosity measurement the rotating body is contactlessly accelerated from the resting position to a certain rotational speed by a cyclic electromagnetic field, which is generated by four induction coils placed outside the measuring cell [4, 5]. When the desired rotational speed is reached, the driving currents are turned off so that no interaction between the rotating body and the drive remains. After shutting off the drive, the rotational speed starts to decrease because of the viscous momentum produced by the fluid.

Since the magnetic coupling serves as a frictionless bearing, the decrease of the speed of rotation is almost completely due to the viscous drag of the fluid. In addition to this, a small residual drag is produced by eddy currents in the electrically conductive measuring cell due to inhomogeneities in the magnetic field of the permanent magnet. This drag is small compared to the viscous drag (even at low viscosities) and can be calibrated very accurately when the measuring cell is evacuated [4, 5].

The rotation speed sensor is placed below the vertical position sensor. It consists of an induction coil and a small magnetic core which is attached to the end of the cylinder and placed about 1 mm outside the center of rotation. The axis of the coil is inclined to about 45° with regard to the rotational axis of the cylinder. When the cylinder rotates, the magnetic core changes the inductivity of the coil depending on the angle of rotation of the cylinder. By means of a special electronic unit, the angle-dependent inductivity of the sensor is transferred into a voltage signal. A clock, similar to a frequency counter, measures the times τ_i needed for each revolution n_i of the cylinder and transfers these data to a computer. The computer stores the periods τ_i and calculates the absolute time t_n corresponding to the nth revolution by adding up the periods τ_i. By this procedure, data pairs of (n, t_n) are generated which allow the analysis of the decay of the rotational speed due to the viscosity of the fluid. Theory predicts [4, 5, 9] that the number of revolutions of the cylinder $n(t)$ varies exponentially with the time t to an asymptotic value n_∞:

$$n(t) = n_\infty [1 - \exp(-Dt)] \tag{2}$$

The characteristic value of Eq. (2) is the so-called damping constant D, which can be interpreted as the relative decrease of the rotational speed. The damping constant D is the quantity calculated from the actual measuring signal $n(t)$ of the viscometer since it is proportional to the viscosity. In order to determine D, Eq. (2) is fitted automatically by the computer to the data pairs (n, t_n).

Equation (2) corresponds directly to the solution of the fluid dynamic model [4, 5, 9] of the viscosity measuring principle, which describes the time-dependent number of revolutions $n(t)$ of the rotating body as follows:

$$n(t) = n_\infty \left[1 - \exp\left(-\frac{\eta C + D_R}{z} t \right) \right]. \tag{3}$$

A comparison between Eqs. (2) and (3) leads to the working equation of the viscosity measuring principle, where the dynamic viscosity η is calculated as

$$\eta = \frac{zD - D_R}{C} \tag{4}$$

The damping constant D_R corrects the measured value of D for the residual drag. The factor C is the so-called apparatus coefficient and z is the nonstationary parameter, which interprets the nonstationary character of the flow as an increase in the moment of inertia of the cylinder due to the rotating fluid [4, 5, 9]. The values of the apparatus coefficient C and the nonstationary parameter z depend mainly on the geometric parameters of the measuring system and the mass of the rotating body. Moreover, the nonstationary parameter z depends also on the density of the surrounding fluid.

The combined viscometer-densimeter covers a viscosity range up to 150 $\mu Pa \cdot s$ and a density range up to 2000 $kg \cdot m^{-3}$ at temperatures from 233 to 523 K and pressures up to 30 MPa.

3. ADVANCEMENT OF THE APPARATUS

The first version of the combined viscometer-densimeter was designed and based on the knowledge and experience we had gained from the density measuring principle [7, 8]. Consequently, right from the beginning, the apparatus achieved uncertainties in density (see Table I) which are of the same order as the uncertainties obtained from the most accurate density measuring apparatus worldwide.

Table I. Specifications of the Viscometer-Densimeter

Measuring quantities	$\eta\rho T(p)$ data in the homogeneous fluid region
Measuring range	
Temperature	$233\ \mathrm{K} \leqslant T \leqslant 523\ \mathrm{K}$
Pressure	up to 30 MPa
Density	up to $2000\ \mathrm{kg \cdot m^{-3}}$
Viscosity	up to $150\ \mu\mathrm{Pa \cdot s}$
Uncertainties of the quantities T, p, and ρ	
Temperature	$\Delta T \leqslant \pm 20\ \mathrm{mK}$
Pressure	$\Delta p/p \leqslant \pm(0.01 + 0.1\ \mathrm{MPa}/p)\%$
Density	$\Delta\rho/\rho \leqslant \pm(0.02 + 0.8\ \mathrm{kg \cdot m^{-3}}/\rho)\%$
Uncertainty of the viscosity	
Residual Damping	$\Delta D_R/(zD - D_R) \leqslant \pm 0.03\%$
Damping	$\Delta D/(zD - D_R) \leqslant \pm 0.024\%$
Nonstationary parameter	$\Delta z/(zD - D_R) \leqslant \pm[0.0015 + 0.001\ \rho/(\mathrm{kg \cdot m^{-3}})]\%$
Apparatus coefficient	$\Delta C/C \leqslant \pm 0.14\%$
Total uncertainty	$\Delta\eta/\eta \leqslant \pm[0.15 + 0.001\ \rho/(\mathrm{kg \cdot m^{-3}})]\%$
Fluids to be measured	Pure fluids and mixtures

The viscosity measuring principle was a new development, and yet it was possible to achieve uncertainties of ± 0.6 to $\pm 1.0\%$ in viscosity [4, 5]. These uncertainties are within the boundaries of common viscosity measuring apparatus (only a few and very special apparatus have so far achieved smaller uncertainties) and very remarkable due to the large working range of the combined viscometer-densimeter. Nevertheless, initially it was necessary to calibrate the viscosity measuring system on a reference fluid in order to achieve the uncertainties mentioned above. Thus, the viscosity measuring principle was not yet absolute and still unsatisfactory with regard to the high quality of the fluid dynamic model that predicted the possibility of absolute measurements as well as smaller uncertainties in viscosity measurements.

3.1. The Fluid Dynamic Model

The fluid dynamic model of the viscosity measuring principle is based on an exact solution to the Navier–Stokes equations and depends only on those parameters of the measuring system, which can be determined very accurately, namely the geometric parameters (diameters and heights of the cylinders), the mass of the rotating body, the density of the surrounding fluid, and the time for each revolution. Therefore, the model can be described very accurately and comprehensively so long as its boundary conditions are observed using a suitably designed viscosity measuring system. The boundary conditions can be considered as follows:

First of all, the flow of the fluid has to be laminar around the rotating body. The laminar flow depends on the rotational speed, on the kinematic viscosity of the fluid, and on the radii of the inner and outer cylinders. In this context and with regard to the large operational range of the viscometer-densimeter, it can be established that the rotational speed should be small and the annulus between the cylinders has to be narrow [4, 5].

Secondly, the fluid dynamic model is valid for concentric cylinders. Thus, displacements of the rotational axis of the rotating body may cause quite large uncertainties in viscosity, especially when the annulus between the cylinders is narrow [4, 5] (which is necessary for the large operational range).

Finally, for the fluid dynamic model the dominating flow is considered the cylindrical flow in the annulus. For this reason the measuring system had to be designed as a long slender cylinder system with low influences of the so-called end flows at the end faces of the rotating body. For the end faces, in general, two flow situations can be taken into account. If the clearance of the housing is sufficiently large, then the flow can be described as a rotating disk in an infinite fluid without any wall effects. Otherwise, the flow has to be described as a disk flow surrounded by a housing with narrow gaps [4, 5]. In both flow cases there are solutions to the Navier–Stokes equations, but—in the sense of the dominating cylinder flow—the free disk flow is preferred due to the greater influence of the disk flow in a housing.

3.2. Improvements in Design

In accordance with the boundary conditions of the fluid dynamic model, some difficulties have been established as being the reason for the necessary calibration of the viscosity measuring system and also for the persisting "high" uncertainties in viscosity of the first version of the viscometer-densimeter [5]. After analyzing the problems, the design of the measuring system of the viscometer-densimeter was improved in such a way that the uncertainty in density measurement is not affected so that the apparatus clearly meets the conditions of the fluid dynamic model. As a result of this, it is now possible to calculate the apparatus coefficients directly from the geometric dimensions of the cylindrical system. Since calibration is no longer necessary, the measuring principle is now applied in an absolute sense. Moreover, the uncertainty in viscosity has significantly decreased.

The difficulties of the first version of the viscometer-densimeter are shown on the left side of Fig. 2. The advanced principle of the viscometer-densimeter can be seen on the right side of Fig. 2.

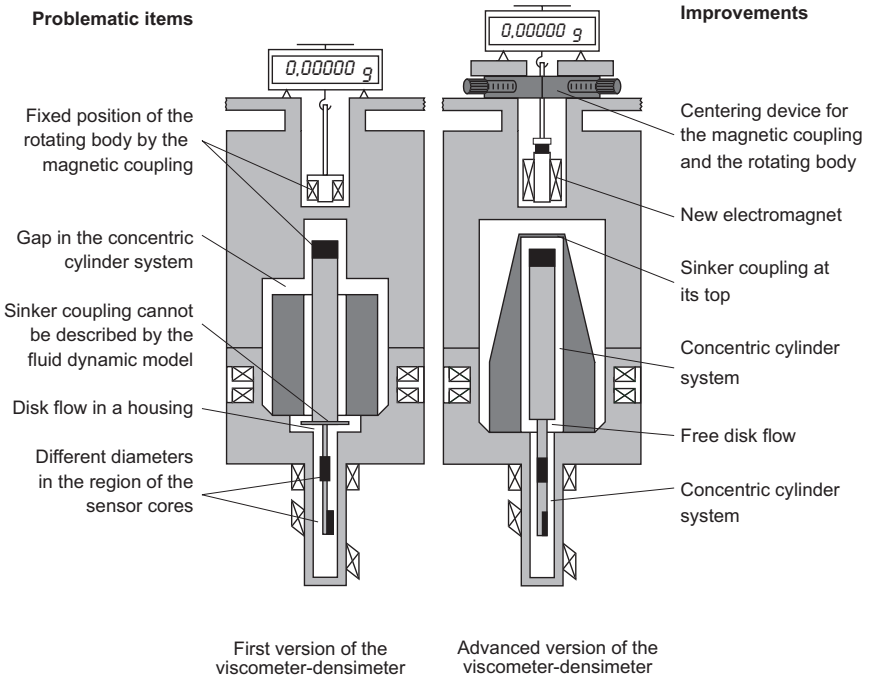

Fig. 2. Comparison between the initial and the advanced viscometer-densimeter.

First of all, a device for centering the cylinder system was embedded into the apparatus. This device is placed below the microbalance outside the measuring cell (see Fig. 2) and is able to move the freely suspended rotating body contactlessly in two orthogonal horizontal directions since the magnetically suspended rotating body centers itself in the magnetic field between the electromagnet and permanent magnet. Therefore, it is sufficient to move the microbalance (including the electromagnet) and the rotating body follows this motion automatically. To control the concentric position of the cylinders, the motion on the orthogonal axis is done in sufficiently small steps of about 10 μm and the damping constant D is measured at each position. According to the fluid dynamic model, the damping is minimal when the concentric position is reached [5]. By using the centering device, an essential part of the uncertainty of the viscosity measurement is eliminated, whereas the density measurement is not affected.

Furthermore, the design of the concentric cylinder system was simplified in order to improve the boundary conditions of the fluid dynamic

model. Consequently, as shown in Fig. 2, the rotating body has been designed as a long slender cylinder. It is surrounded by the new sinker along the whole height. Since the sinker coupling is no longer part of the rotating body but of the sinker itself, the sinker is now coupled at its top for density measurements. Due to the new design of the cylinder system, there are no longer flow regions that cannot be described by the fluid dynamic model. In particular, the errors caused by the gap between the sinker and the measuring cell and by the sinker coupling have been eliminated.

In order to guarantee free disk flows at both faces of the rotating body, it was necessary to suspend the rotating body at a lower vertical position. In general, the distance of the magnetic system (electromagnet and permanent magnet) corresponds to the equilibrium between the magnetic force and the weight acting on the magnetic coupling. Thus, a new, stronger electromagnet was integrated into the apparatus. The new electromagnet is larger than the old one and has an additional permanent magnet embedded in its ferritic core. Since the magnetic coupling now has a stronger field, the rotating body is suspended in a lower vertical position and the disk flows can be described as free disk flows with a sufficiently small influence on the entire flow field. Although it was not the original aim, the new magnetic coupling causes a 75% smaller residual drag compared to the first version of the viscometer-densimeter because of fewer inhomogeneities in the magnetic field.

To sum up, it can be said that the improvements to the viscometer-densimeter have not affected the excellent uncertainty in density measurement while the uncertainty in viscosity measurements has been reduced enormously and is only dependent on the parameters of the fluid dynamic model. Moreover, the measuring system clearly meets the boundary conditions of the fluid dynamic model. Therefore, it is now possible to calculate the apparatus coefficients and the nonstationary parameters directly from the geometric dimensions of the cylindrical system, the mass of the rotating body and the density of the fluid. Since calibration is no longer necessary, the measuring principle is now absolute.

3.3. Specifications of the Advanced Viscometer-Densimeter

Table I summarizes the specifications of the advanced apparatus, which is designed to measure viscosity-density-temperature data ($\eta\rho T$ data) in the homogeneous fluid region. The measuring range covers temperatures from 233 to 523 K and pressures up to 30 MPa, densities up to 2000 $kg \cdot m^{-3}$, and viscosities up to 150 $\mu Pa \cdot s$. The operational range given here only relates to this apparatus and not to the principle of viscosity measurements in general.

The uncertainties in temperature and density are small compared with the uncertainty in viscosity, thus guaranteeing $\eta\rho T$ data sets of high consistency. The pressure is—in the sense of $\eta\rho T$ measurements—only measured for completeness. The uncertainty of the viscosity measurement is estimated by applying the Gaussian error-propagation formula to the working equation, Eq. (4), of the viscometer. The single error sources are listed in Table I. The list also contains the uncertainty introduced by the calibration of the residual damping constant D_R, the uncertainty of the measurement of the damping constant D, and the uncertainties of the calculation of the apparatus coefficient C and the calculation of the nonstationary parameter z. The greatest constant part of the uncertainty results from the apparatus coefficient C. The part of the uncertainty which is proportional to the density of the fluid results from the uncertainty of the nonstationary parameter z.

4. MEASUREMENTS ON NITROGEN, ARGON, METHANE, HELIUM, NEON, AND KRYPTON

After a careful examination of the advanced viscometer-densimeter, comprehensive $\eta\rho T$ measurements on nitrogen (81 values), argon (72 values), and methane (61 values) were carried out on 8 isotherms each in the temperature range from 233 to 523 K. Moreover, measurements on helium (34 values), neon (16 values), and krypton (18 values) were carried out on the isotherms 298.15 (293.15 for helium) and 348.15 K. To check the reproducibility of the results, some of the measurements were repeated at selected points at different times.

4.1. Results

The experimental results for the six fluids are listed in Tables II to VII. As mentioned previously, the pressure values in these tables were measured only for completeness.

The substances nitrogen, argon, methane, and helium used for the measurements were supplied by Linde, Germany. The certified purity of the nitrogen was $x(N_2) > 0.999995$ [impurities: $x(O_2) \leqslant 2 \times 10^{-6}$, $x(H_2O) \leqslant 2 \times 10^{-6}$, and $x(C_mH_n) \leqslant 1 \times 10^{-7}$, where x denotes mole fraction]. The purity of the argon was $x(Ar) > 0.999996$ [impurities: $x(O_2) \leqslant 7 \times 10^{-7}$, $x(N_2) \leqslant 1 \times 10^{-6}$, $x(H_2O) \leqslant 1 \times 10^{-6}$, and $x(C_mH_n) \leqslant 1 \times 10^{-7}$, where x denotes mole fraction] and the purity of the methane was $x(CH_4) > 0.999992$ [impurities: $x(O_2) \leqslant 5 \times 10^{-7}$, $x(N_2) \leqslant 4 \times 10^{-6}$, $x(H_2O) \leqslant 2 \times 10^{-6}$, $x(H_2) \leqslant 1 \times 10^{-7}$, and $x(C_mH_n) \leqslant 5 \times 10^{-7}$, where x denotes mole fraction]. The purity of the helium was $x(He) > 0.99996$ [impurities: $x(O_2) \leqslant 5 \times 10^{-6}$, $x(N_2) \leqslant 2 \times 10^{-5}$, $x(H_2O) \leqslant 5 \times 10^{-6}$, and $x(C_mH_n) \leqslant 1 \times 10^{-6}$, where x denotes mole fraction].

Table II. New $\eta\rho T$ Results for Nitrogen, where η is the Viscosity, ρ is the Density, T is the Temperature (ITS-90), and p is the Pressure

p (MPa)	ρ ($kg \cdot m^{-3}$)	η ($\mu Pa \cdot s$)	p (MPa)	ρ ($kg \cdot m^{-3}$)	η ($\mu Pa \cdot s$)	p (MPa)	ρ ($kg \cdot m^{-3}$)	η ($\mu Pa \cdot s$)
				$T = 233.15$ K				
0.106	1.535	14.701	5.879	89.687	16.217	11.613	180.224	18.817
2.002	29.558	15.078	7.830	120.714	16.992	13.574	209.739	19.885
3.981	59.849	15.598	9.683	150.138	17.834	15.708	240.226	21.110
				$T = 263.15$ K				
0.115	1.474	16.162	9.128	119.927	18.430	16.330	209.659	21.338
2.320	30.066	16.548	11.422	149.611	19.280	18.981	239.420	22.528
4.587	59.950	17.062	13.694	178.048	20.204	21.918	270.162	23.886
6.842	89.839	17.688						
				$T = 293.15$ K				
0.098	1.131	17.563	10.485	120.265	19.858	22.370	240.283	23.993
0.116	1.348	17.577	13.196	149.884	20.707	25.746	269.218	25.254
2.602	30.053	17.961	13.210	150.029	20.803	29.702	300.215	26.717
5.185	59.960	18.475	16.167	180.960	21.715	29.736	300.361	26.731
7.801	90.014	19.106	19.117	210.153	22.775			
				$T = 333.15$ K				
0.101	1.018	19.369	9.060	90.015	20.899	19.037	180.133	23.475
2.983	30.083	19.760	12.245	120.130	21.649	22.740	210.098	24.557
5.988	60.033	20.270	15.553	150.132	22.501	26.683	239.785	25.741
				$T = 373.15$ K				
0.103	0.915	21.073	10.320	90.099	22.605	21.956	180.096	25.177
0.125	1.144	21.078	13.979	119.947	23.327	26.302	209.887	26.247
3.359	30.086	21.461	13.991	120.051	23.346	26.329	210.063	26.262
6.807	60.270	21.982	17.858	150.072	24.205			
				$T = 423.15$ K				
0.127	1.023	23.117	11.669	88.608	24.611	20.715	149.981	26.240
3.822	30.034	23.504	16.146	119.853	25.381	25.615	180.298	27.223
7.763	60.020	24.017						
				$T = 473.15$ K				
0.134	0.968	25.030	13.417	90.027	26.556	23.570	150.002	28.152
4.288	30.023	25.415	18.336	119.984	27.298	29.168	180.015	29.126
8.748	60.034	25.926						
				$T = 523.15$ K				
0.143	0.919	26.846	9.702	59.876	27.733	20.482	119.893	29.106
0.157	1.028	26.840	14.928	89.830	28.361	26.399	149.971	29.959
4.752	29.998	27.195	15.001	90.247	28.375	26.460	150.244	29.972

Table III. New $\eta\rho T$ Results for Argon, where η is the Viscosity, ρ is the Density, T is the Temperature (ITS-90), and p is the Pressure

p (MPa)	ρ (kg·m^{-3})	η (μPa·s)	p (MPa)	ρ (kg·m^{-3})	η (μPa·s)	p (MPa)	ρ (kg·m^{-3})	η (μPa·s)
				$T = 233.15$ K				
0.121	2.314	18.285	4.073	90.690	19.536	7.666	180.007	21.390
1.404	29.643	18.614	5.313	120.004	20.087	8.793	210.053	22.145
2.778	60.064	19.045	6.510	150.033	20.708	9.652	238.897	22.777
				$T = 263.15$ K				
0.101	1.844	20.376	4.699	90.034	21.650	9.053	180.194	23.536
1.616	30.014	20.721	6.182	120.147	22.214	10.460	210.210	24.297
3.180	60.470	21.152	7.624	150.055	22.840	11.853	240.099	25.367
				$T = 293.15$ K				
0.096	1.575	22.312	5.315	89.978	23.098	10.417	180.121	25.473
0.100	1.636	22.321	5.321	90.078	23.589	12.094	210.009	26.229
1.811	30.040	22.661	7.035	120.096	24.152	13.782	239.976	27.039
3.582	60.062	23.092	8.726	150.031	24.777	13.784	240.006	27.053
				$T = 333.15$ K				
0.094	1.357	24.789	6.147	90.078	26.069	12.219	179.985	27.950
2.068	30.011	25.141	8.169	120.062	26.631	14.281	210.172	28.715
4.114	60.042	25.572	10.191	150.052	27.258	16.511	242.366	29.606
				$T = 373.15$ K				
0.096	1.236	27.142	6.968	90.054	28.436	14.020	180.025	30.318
0.102	1.314	27.156	7.005	90.548	28.514	16.431	210.019	31.076
2.325	30.010	27.507	9.294	119.988	28.997	18.854	239.645	31.889
4.644	60.007	27.938	11.646	150.053	29.625	19.036	241.813	31.952
				$T = 423.15$ K				
0.097	1.102	29.946	8.041	90.593	31.237	16.253	179.993	33.110
2.645	29.991	30.297	10.734	120.365	31.796	19.109	209.949	33.867
5.306	59.992	30.730	13.456	150.036	32.418	22.034	239.869	34.689
				$T = 473.15$ K				
0.998	1.013	32.555	9.008	89.995	33.863	18.467	179.921	35.716
2.967	29.987	32.908	12.084	119.944	34.395	21.763	209.823	36.474
5.962	59.941	33.339	15.249	149.968	35.025	24.983	238.270	37.252
				$T = 523.15$ K				
0.109	1.000	34.982	10.011	89.878	36.261	20.672	179.904	38.143
0.111	1.020	34.995	10.029	90.031	36.310	24.411	209.853	38.901
3.287	29.981	35.336	13.487	119.941	36.824	27.928	237.208	39.648
6.625	59.977	35.766	17.027	149.841	37.449	28.139	238.827	39.694

Table IV. New $\eta\rho T$ Results for Methane, where η is the Viscosity, ρ is the Density, T is the Temperature (ITS-90), and p is the Pressure

p (MPa)	ρ (kg·m^{-3})	η (μPa·s)	p (MPa)	ρ (kg·m^{-3})	η (μPa·s)	p (MPa)	ρ (kg·m^{-3})	η (μPa·s)
				$T = 233.15$ K				
0.127	1.052	8.941	8.837	119.592	14.197	14.301	210.397	22.679
3.152	30.040	9.743	10.345	150.525	16.581	17.759	240.235	26.631
5.515	60.070	10.880	12.005	180.153	19.332	23.235	269.487	31.278
7.338	90.078	12.361						
				$T = 263.15$ K				
0.128	0.933	9.969	9.349	90.170	13.422	17.383	180.437	20.308
3.692	30.058	10.798	11.772	119.836	15.250	21.300	210.339	23.547
6.724	60.078	11.940	14.353	150.168	17.546	25.643	234.626	26.568
				$T = 293.15$ K				
0.151	0.990	10.979	11.298	89.924	14.428	22.676	179.992	21.211
0.163	1.073	10.977	11.310	90.033	14.442	28.108	209.359	24.304
4.219	30.017	11.807	14.702	120.156	16.293	28.246	210.062	24.382
7.912	60.058	12.966	18.351	150.057	18.535			
				$T = 333.15$ K				
0.171	0.985	12.261	13.907	90.042	15.768	23.650	150.080	19.829
4.911	29.955	13.106	18.521	120.083	17.608	29.674	179.669	22.428
9.470	60.022	14.279						
				$T = 373.15$ K				
0.189	0.975	13.479	10.985	59.841	15.531	22.229	119.693	18.854
0.195	1.002	13.482	16.440	89.847	17.028	28.850	149.878	21.067
5.597	29.907	14.346	16.479	90.055	17.047	28.881	150.001	21.079
				$T = 423.15$ K				
0.210	0.954	14.901	12.902	59.858	17.023	26.961	119.920	20.384
6.462	29.917	15.812	19.598	89.791	18.534			
				$T = 473.15$ K				
0.227	0.922	16.280	14.805	59.881	18.379	22.793	89.973	19.872
7.313	29.885	17.165						
				$T = 523.15$ K				
0.261	0.959	17.577	8.285	30.304	18.482	25.861	89.769	21.154
0.272	1.001	17.590	16.612	59.592	19.656	25.963	90.075	21.177

Table V. New $\eta\rho T$ Results for Helium, where η is the Viscosity, ρ is the Density, T is the Temperature (ITS-90), and p is the Pressure

p (MPa)	ρ (kg·m^{-3})	η (μPa·s)	p (MPa)	ρ (kg·m^{-3})	η (μPa·s)	p (MPa)	ρ (kg·m^{-3})	η (μPa·s)
				$T = 293.15$ K				
0.123	0.200	19.612	0.857	1.397	19.611	3.716	5.993	19.613
0.123	0.199	19.612	0.979	1.602	19.611	4.985	8.001	19.611
0.244	0.397	19.612	1.101	1.802	19.612	6.308	10.058	19.614
0.366	0.604	19.614	1.226	2.005	19.612	6.500	10.359	19.612
0.489	0.803	19.611	1.241	2.026	19.612	7.572	12.003	19.612
0.610	1.002	19.614	1.843	3.002	19.611	8.781	13.851	19.609
0.618	1.007	19.612	2.465	4.004	19.614	9.540	14.996	19.610
0.734	1.198	19.614	2.467	4.005	19.612			
				$T = 348.15$ K				
0.145	0.200	22.067	0.869	1.200	22.065	2.836	3.874	22.066
0.146	0.203	22.067	1.017	1.404	22.067	2.911	3.979	22.067
0.290	0.404	22.067	1.160	1.597	22.068	4.410	5.996	22.067
0.435	0.597	22.067	1.305	1.800	22.066	5.912	7.994	22.065
0.580	0.801	22.068	1.455	2.000	22.067	7.427	9.978	22.067
0.724	0.995	22.067	1.456	2.000	22.067	7.438	9.991	22.067
0.726	0.998	22.067	2.187	3.000	22.068	8.875	11.867	22.064

The neon used for the measurements was supplied by Messer Griesheim, Germany, with a certified purity of $x(\mathrm{Ne}) > 0.99998$ [impurities: $x(\mathrm{O_2}) \leqslant 1 \times 10^{-6}$, $x(\mathrm{N_2}) \leqslant 2 \times 10^{-6}$, $x(\mathrm{H_2O}) \leqslant 2 \times 10^{-6}$, $x(\mathrm{C_mH_n}) \leqslant 1 \times 10^{-7}$, and $x(\mathrm{He}) \leqslant 5 \times 10^{-6}$, where x denotes mole fraction].

The krypton used for the measurements was supplied by Air Products, Germany, with a certified purity of $x(\mathrm{Kr}) > 0.99997$ [impurities $x(\mathrm{O_2}) \leqslant 1 \times 10^{-6}$, $x(\mathrm{N_2}) \leqslant 5 \times 10^{-6}$, $x(\mathrm{H_2O}) \leqslant 3 \times 10^{-6}$, $x(\mathrm{C_mH_n}) \leqslant 1 \times 10^{-6}$, $x(\mathrm{H_2}) \leqslant 1 \times 10^{-7}$, $x(\mathrm{Xe}) \leqslant 3 \times 10^{-6}$, and $x(\mathrm{Ar}) \leqslant 2 \times 10^{-6}$, where x denotes mole fraction].

The experimental uncertainties of the individual quantities η, ρ, and T have already been discussed in Section 3. The total uncertainty of the $\eta\rho T$ measurement was calculated on the basis of the single uncertainties by applying the Gaussian error-propagation formula. Since the uncertainties in temperature and density are small compared with the uncertainty in viscosity and since the density and temperature dependence of every investigated fluid is quite weak, the total uncertainty of the $\eta\rho T$ measurement does not exceed the uncertainty in viscosity listed in Table I.

Table VI. New $\eta\rho T$ Results for Neon, where η is the Viscosity, ρ is the Density, T is the Temperature (ITS-90), and p is the Pressure

p (MPa)	ρ (kg·m^{-3})	η (μPa·s)	p (MPa)	ρ (kg·m^{-3})	η (μPa·s)	p (MPa)	ρ (kg·m^{-3})	η (μPa·s)
				$T = 298.15$ K				
0.101	0.818	31.691	0.995	8.064	31.728	7.998	62.678	32.142
0.201	1.634	31.697	4.003	31.976	31.900	12.051	92.697	32.415
0.401	3.257	31.721	4.007	32.005	31.902	15.827	119.641	32.674
				$T = 348.15$ K				
0.101	0.702	35.225	1.001	6.948	35.267	7.995	53.859	35.635
0.200	1.393	35.261	3.980	27.270	35.412	11.986	79.406	35.842
0.402	2.795	35.252	4.010	27.477	35.424	15.732	102.609	36.048

4.2. Discussion

4.2.1. Nitrogen

A brief comparison of the new $\eta\rho T$ data on nitrogen (see Table II) with several selected measurements of other authors is presented in Fig. 3. The diagrams show the percentage deviations between measured values and values calculated from the $\eta\rho T$ correlation equation of Stephan et al. [10]. The experimental results of other authors were considered, but not selected for comparison because of wide scatter, systematic deviations, and a small

Table VII. New $\eta\rho T$ Results for Krypton, where η is the Viscosity, ρ is the Density, T is the Temperature (ITS-90), and p is the Pressure

p (MPa)	ρ (kg·m^{-3})	η (μPa·s)	p (MPa)	ρ (kg·m^{-3})	η (μPa·s)	p (MPa)	ρ (kg·m^{-3})	η (μPa·s)
				$T = 298.15$ K				
0.100	3.384	25.379	3.013	108.517	26.509	6.005	231.165	28.364
0.101	3.389	25.387	4.016	148.044	27.042	6.999	275.515	29.181
1.003	34.809	25.673	4.072	150.092	27.074	7.951	319.942	30.048
2.024	71.314	26.061	5.011	188.673	27.655			
				$T = 348.15$ K				
0.099	2.854	29.131	3.013	90.305	30.035	6.002	186.026	31.369
0.101	2.900	29.133	3.997	121.146	30.427	7.016	219.880	31.923
1.001	29.288	29.372	4.003	121.328	30.430	8.543	271.853	32.851
2.002	59.285	29.679	4.916	150.576	30.832			

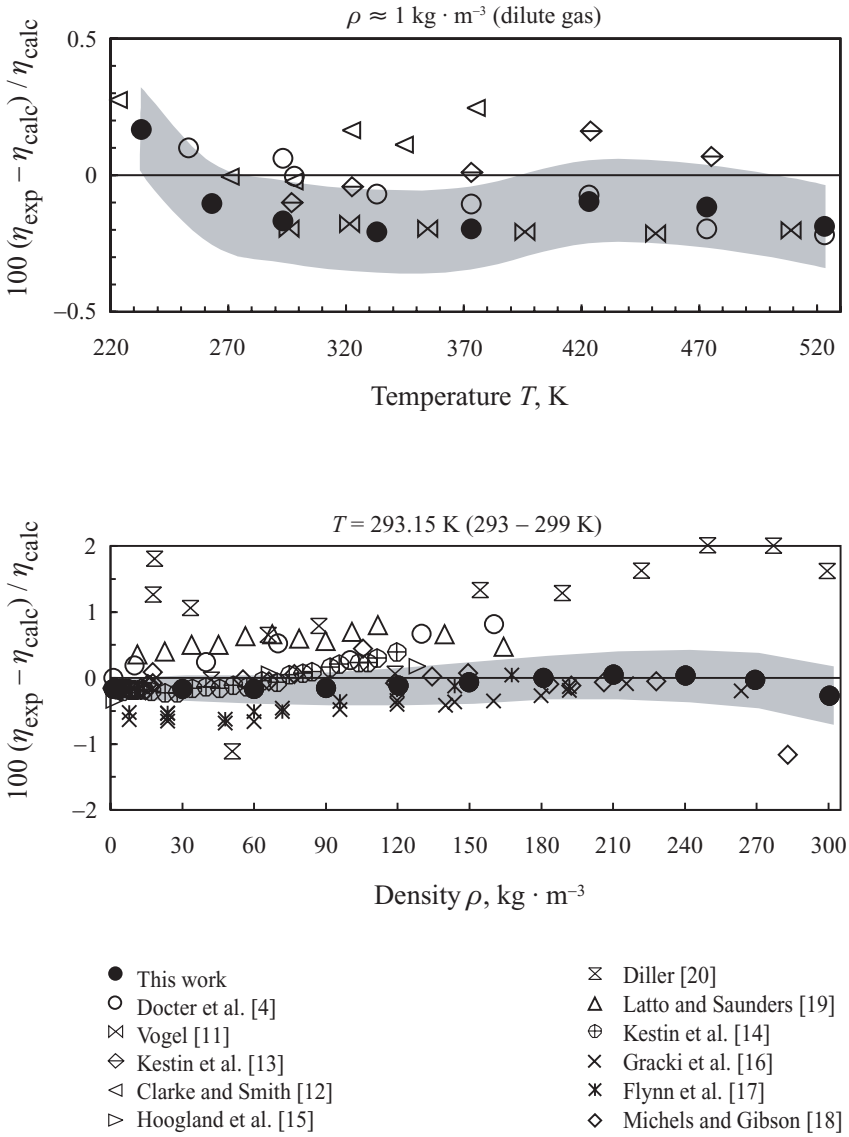

Fig. 3. Measurements of $\eta\rho T$ data of nitrogen with the advanced apparatus in comparison with the experimental viscosities of other authors and with values (zero line) calculated from the correlation equation for the viscosity of nitrogen [10]. The shaded area corresponds to the experimental uncertainty of the measurements in this work.

number of measured points. The uncertainty of the new $\eta\rho T$ data is also illustrated in the deviation diagrams.

The upper diagram in Fig. 3 shows the $\eta\rho T$ data in the dilute gas region by covering the entire operational range in temperature of the viscometer-densimeter from 233 to 523 K. For low and high temperatures the new data agree with the values from the correlation equation [10] within the uncertainty of the new data, while for medium temperatures the deviations of the calculated values are slightly outside the uncertainty. It can be seen that the new data agree well with the measurements of Vogel [11] over the whole temperature range and, except at room temperature, with the measurements of Docter et al. [5], which were carried out with the initial version of the viscometer-densimeter. The data of Clarke and Smith [12] show deviations up to +0.5%. The measuring runs of Kestin et al. [13] deviate up to 0.3% but, at room temperature, the agreement with the new $\eta\rho T$ data is very good.

The lower diagram in Fig. 3 shows viscosity data measured on the 293.15 K isotherm over a wide density range. The temperature value given above the diagram corresponds to the new measurements, and the temperature range written in parentheses covers the results of the other authors. The new data agree quite well with the values calculated from the correlation equation [10]; only in the case of low densities are the calculated values not within the uncertainty of the new data (compare also the upper diagram of Fig. 3). For low and medium densities the new $\eta\rho T$ data are confirmed by those measurements, which were considered as the most accurate $\eta\rho T$ data for nitrogen so far, namely the data set of Kestin et al. [14]. Quite good agreements, with some exceptions in consistency and systematic deviation, exist with the measured values of Hoogland et al. [15], Gracki et al. [16], Flynn et al. [17], and Michels and Gibson [18]. The data set of Latto and Saunders [19] differs systematically from the new $\eta\rho T$ data with deviations up to $\pm 0.9\%$. While the data of Docter et al. [5], measured with the initial version of the viscometer, agree quite well with the new data at low densities the systematic deviation increases up to +1.0% for higher densities. This behavior results from the calibration of the apparatus coefficient and shows the effectiveness of the improvement of the viscometer-densimeter.

4.2.2. Argon

Analogous to nitrogen the new $\eta\rho T$ data on argon (see Table III) are compared with selected measurements of other authors in Fig. 4. The diagrams show the percentage deviations between measured or calculated values and values calculated from the $\eta\rho T$ correlation equation of Younglove and Hanley [21].

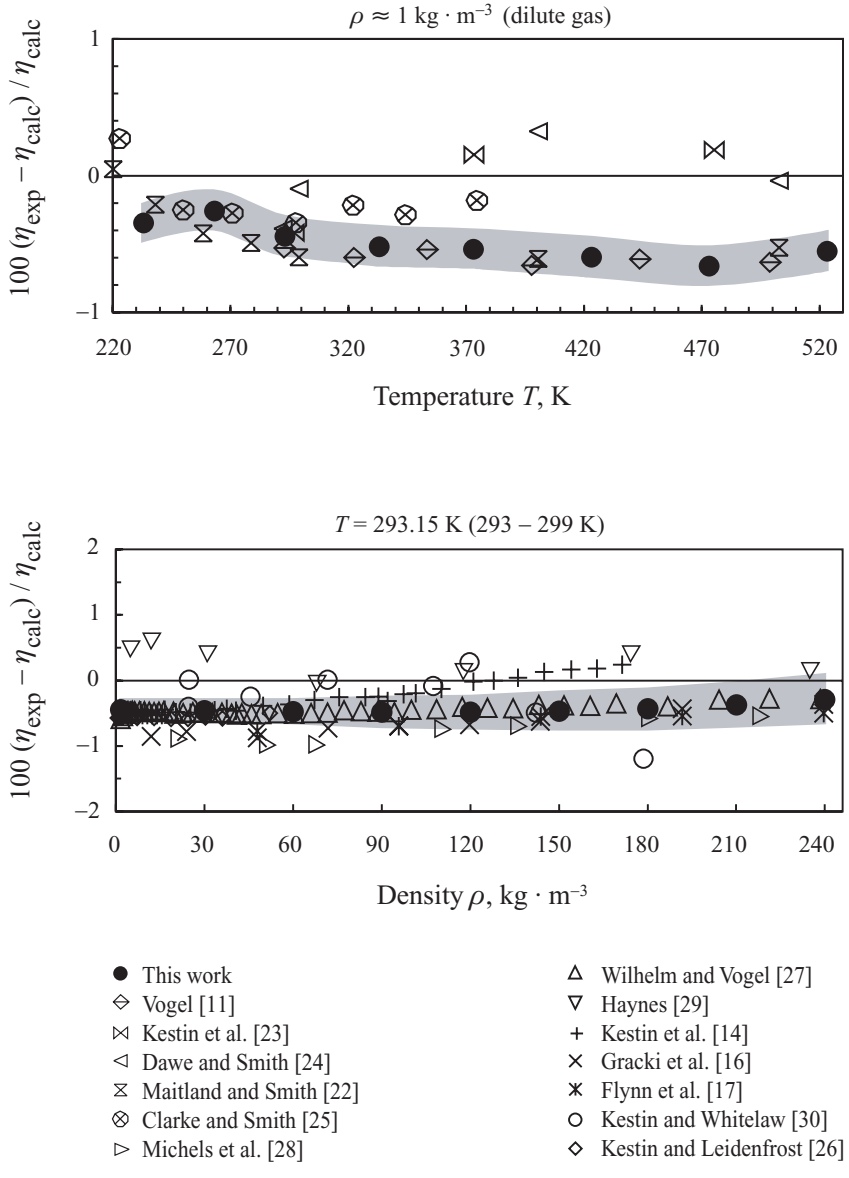

Fig. 4. Measurements of $\eta\rho T$ data of argon with the advanced apparatus in comparison with the experimental viscosities of other authors and with values (zero line) calculated from the correlation equation for the viscosity of argon [21]. The shaded area corresponds to the experimental uncertainty of the measurements in this work.

The upper diagram in Fig. 4 shows the $\eta\rho T$ data in the dilute gas region in the temperature range from 233 to 523 K. The new data cannot be described by the correlation equation [21] within the uncertainty of the new data. The deviations are less than +0.8%, which is still within the uncertainty of the correlation equation [21].

The new data agree within their estimated uncertainty with the measurements of Vogel [11] and the calculated values of Maitland and Smith [22] over the whole temperature range. At room temperature the new data are also confirmed by the measurements of Kestin et al. [23], Dawe and Smith [24], and Clarke and Smith [25], but for other temperatures the deviations of the data of these authors increase.

The lower diagram in Fig. 4 shows viscosity data measured on the 293.15 K isotherm over a wide density range. As shown before for nitrogen for low and medium densities, the new $\eta\rho T$ data are confirmed by the accurate $\eta\rho T$ data of Kestin et al. [14] and, moreover, by the data of Kestin and Leidenfrost [26]. Very good agreement over the whole density range exists with the measured values of Wilhelm and Vogel [27], which can be considered as the most accurate $\eta\rho T$ data [estimated uncertainty: $\leqslant \pm(0.2 \text{ to } 0.3)\%$] besides this work. Nevertheless, the data of the other authors mentioned above have not been measured using absolute measuring principles [14, 26, 27]. The data sets of Gracki et al. [16], Flynn et al. [17], and Michels et al. [28] generally agree with the new data but because of inhomogeneities these data cannot be confirmed within the uncertainty of the new data over the whole density range. The data sets of Haynes [29] and Kestin and Whitelaw [30] scatter around the new data with deviations up to $\pm 1\%$.

4.2.3. Methane

A brief comparison of the new $\eta\rho T$ data on methane (see Table IV) with several selected measurements of other authors is presented in Fig. 5. The baseline for the comparison is calculated from the $\eta\rho T$ correlation equation for methane of Friend et al. [31].

In the upper diagram in Fig. 5 it can be seen that the new $\eta\rho T$ data in the dilute gas region can be described by the correlation equation [31] within the uncertainty of the new data over the entire temperature range. With one exception each, the agreement with the data sets of Kestin and Ro [33] and Clarke and Smith [12] is also within the uncertainty of the new data. The calculated values of Maitland and Smith [22] confirm the new data at low temperatures but deviate up to -0.5% at higher temperatures.

The lower diagram in Fig. 5 again shows viscosity data measured on the 293.15 K isotherm over a wide density range. The correlation equation

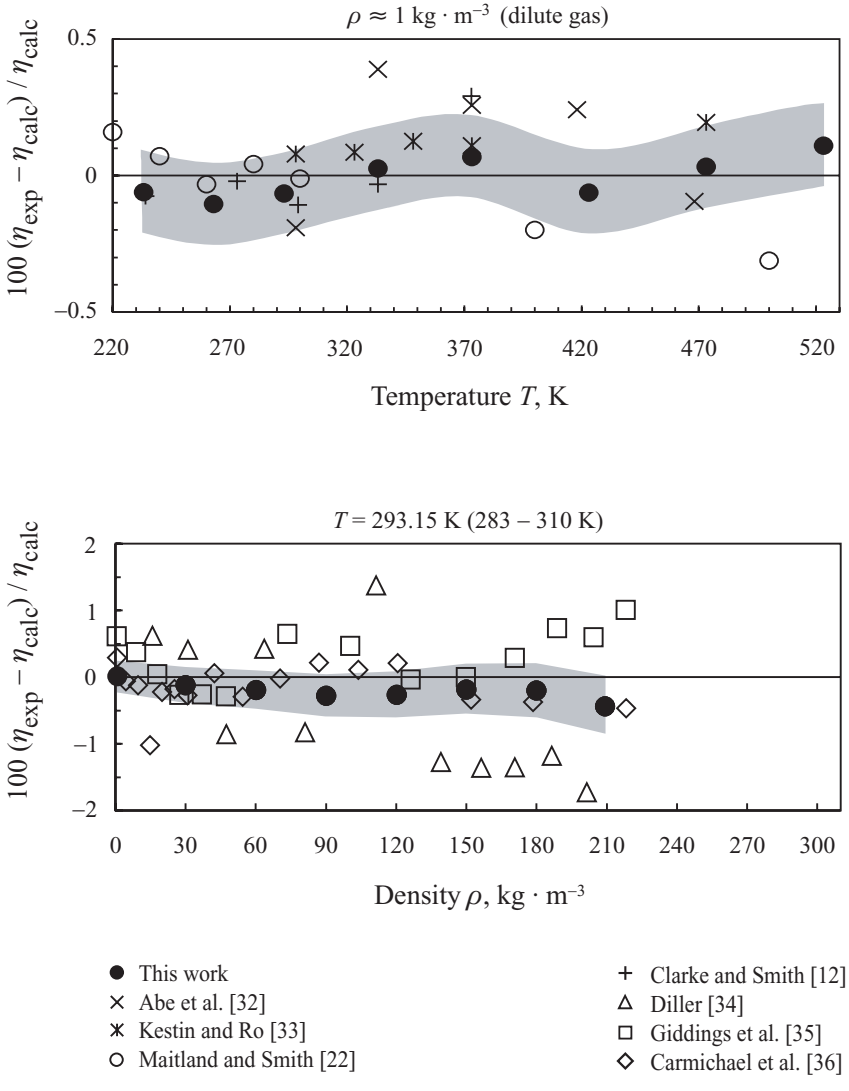

Fig. 5. Measurements of $\eta\rho T$ data of methane with the advanced apparatus in comparison with the experimental viscosities of other authors and with values (zero line) calculated from the correlation equation for the viscosity of methane [31]. The shaded area corresponds to the experimental uncertainty of the measurements in this work.

[31] is able to describe the new $\eta\rho T$ data of methane within their uncertainty. Quite good agreement is also observed with the measured values of Carmichael et al. [36], in general, but some of them are not confirmed within the uncertainty of the new data. The data sets of Diller [34] and Giddings et al. [35] scatter around the new data with deviations up to $\pm 1.8\%$.

4.2.4. Helium

Figure 6 presents a comparison between the new results (see Table V) and selected results of other authors on the 293.15 K isotherm. The zero line corresponds to values calculated from a special regression function. The density dependence of this regression function was fitted to the new data set for helium while the temperature dependence was fitted to very accurate values of Hurly and Moldover [37] gained from *ab initio* calculations. Almost every data set shown in Fig. 6 agrees with the new data within their uncertainty. The agreement of the new data with the very accurately measured values of Vogel [11] and calculated values of Hurly and Moldover [37] is very remarkable with deviations of less than

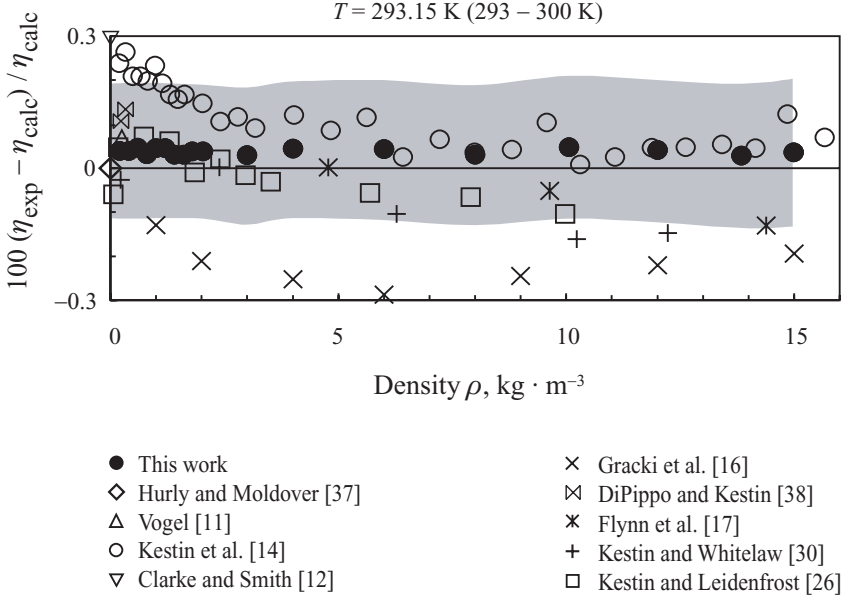

Fig. 6. Measurements of $\eta\rho T$ data of helium with the advanced apparatus in comparison with the experimental viscosities of other authors and with values (zero line) calculated from a regression function fitted to the new data for helium and values calculated by Hurly and Moldover [37]. The shaded area corresponds to the experimental uncertainty of the measurements in this work.

$\pm 0.03\%$. With the exception of very low densities, the deviation of the results of Kestin et al. [14] does not exceed the uncertainty of the new data. Moreover, the data sets of Kestin and Leidenfrost [26] and Flynn et al. [17] can be confirmed.

4.2.5. Neon

A comparison between the new results (see Table VI) and selected results of other authors for neon on the 298.15 K isotherm is presented in Fig. 7. The diagram shows the percentage deviations between measured values and values calculated from the $\eta\rho T$ correlation equation for neon of Rabinovich et al. [39]. Except for low densities the correlation equation is able to describe the new data within their uncertainty. Nevertheless, the equation seems to predict a different density dependence than the new data. The data set of Flynn et al. [17] agrees very well with the new data over the entire density range. The results of the other authors exist only up to medium densities. The data of Kestin and Nagashima [40], DiPippo and Kestin [38], Kestin and Leidenfrost [26], and Vogel [11] are partly confirmed by the new data within their uncertainty but, in general, the

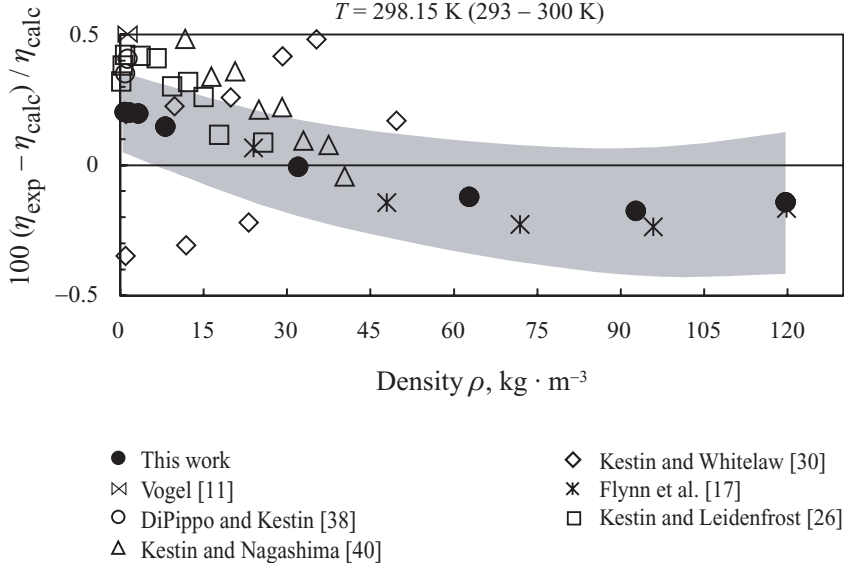

Fig. 7. Measurements of $\eta\rho T$ data of neon with the advanced apparatus in comparison with the experimental viscosities of other authors and with values (zero line) calculated from the correlation equation for the viscosity of neon [39]. The shaded area corresponds to the experimental uncertainty of the measurements in this work.

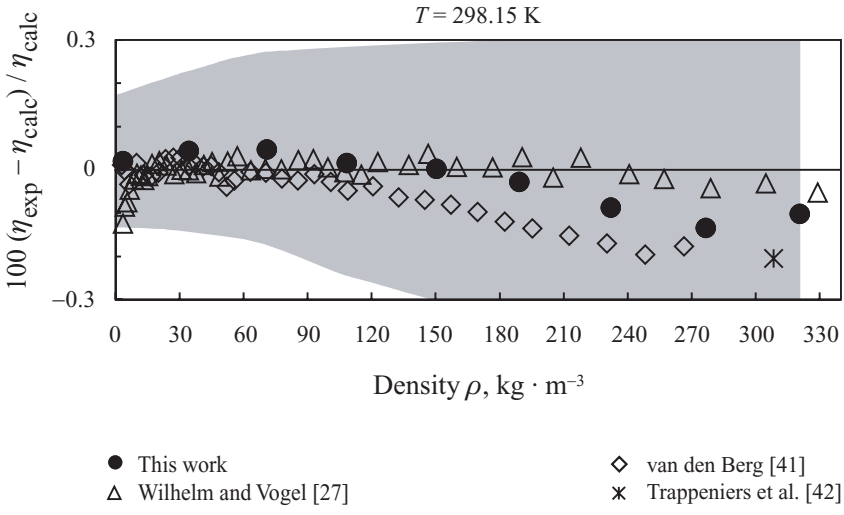

Fig. 8. Measurements of $\eta\rho T$ data of krypton with the advanced apparatus in comparison with the experimental viscosities of other authors and with values (zero line) calculated from a regression function of Wilhelm and Vogel [27] fitted to their measuring results for krypton. The shaded area corresponds to the experimental uncertainty of the measurements in this work.

deviations are within $\pm 0.3\%$. The heavily scattered data of Kestin and Whitelaw [30] deviate up to $\pm 0.7\%$ from the new data.

4.2.6. Krypton

Figure 8 presents a comparison between the new results of krypton (see Table VII) and a few but accurate results of other authors on the 298.15 K isotherm. The zero line corresponds to values calculated from a regression function of Wilhelm and Vogel [27] fitted to their data set.

Notably, all of the data of the other authors agree excellently with the new data within their uncertainty. The maximum deviation of the results of Wilhelm and Vogel [27], van den Berg [41], and Trappeniers et al. [42] is less than $\pm 0.1\%$.

5. NEW, SPECIAL APPARATUS FOR VERY ACCURATE VISCOSITY MEASUREMENTS AT LOW DENSITIES

In the preceding section it can be seen that the measured results carried out with the combined viscometer-densimeter already verifies its capability and that the estimated uncertainty is reliable and on the highest level worldwide—especially with regard to the large operational range of the viscometer-densimeter.

However, when the viscometer-densimeter was improved it was found that at certain conditions the viscosity measuring principle has the capability of achieving even lower uncertainties in viscosity. Theoretical examinations have led to the conclusion, that the uncertainty in viscosity can be minimized when the viscometer works as a single instrument in the limit of low densities. On this basis, a special, and highly accurate apparatus was designed. The viscosity measurements carried out with this apparatus were used to confirm the results of the combined viscometer-densimeter.

5.1. Description of the Apparatus

Figure 9 shows a schematic of the special apparatus for viscosity measurements at low densities. The viscosity measuring principle is the same as in the combined viscometer-densimeter (see Section 2). Again, the rotating body is placed in a concentric cylinder system. Since no density measurement is intended, the outer cylinder is identical with the inner wall of the measuring cell. Due to the small operational range in density, the annulus

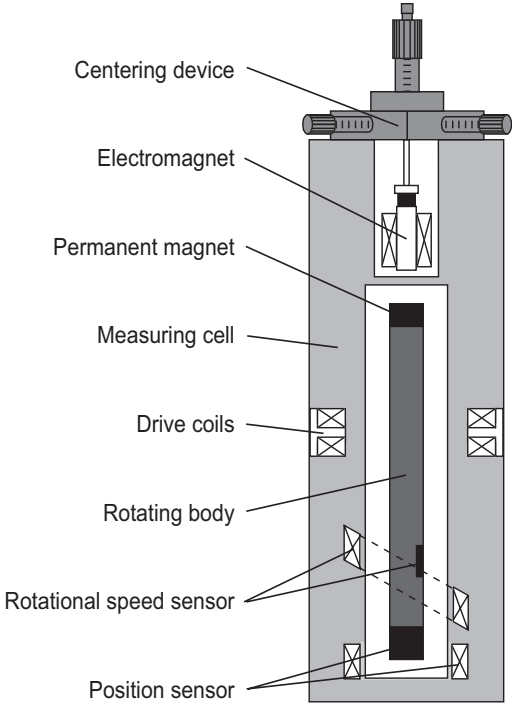

Fig. 9. Principle of the special viscometer for low densities.

of the concentric cylinder system is larger than in the combined viscometer-densimeter, thus guaranteeing that errors caused by any eccentric displacement of the rotational axis are negligible. Nevertheless, a centering device similar to the combined viscometer-densimeter is integrated in the apparatus. Since no balance is needed, the electromagnet is directly attached to the centering device. Although a very strong magnetic coupling is not really necessary, an electromagnet similar to the one used in the advanced viscometer-densimeter is used in the special apparatus due to the reduced residual drag. Moreover, the residual drag was almost eliminated by choosing a titanium alloy (Ti6Al4V) as material for the measuring cell. The titanium alloy has a very low electrical conductivity, so eddy currents induced by inhomogeneities of the magnetic field of the rotating permanent magnet are very weak. The rotating body is optimized with regard to the fluid dynamic model. It is designed as a long slender cylinder, and the ferromagnetic cores of the position sensor and the rotation speed sensor are embedded directly into the main body.

Since the special apparatus has been optimized due to the fluid dynamic model, the total uncertainty of the viscosity measurements can be estimated to be less than $\pm 0.07\%$. Again, this uncertainty only depends on the uncertainties of the basic parameters of the measuring system (geometric parameters, mass of the rotating body, and time measurement). Thus, the special apparatus is also an absolute measuring instrument.

5.2. Measurements on Nitrogen, Argon, Helium, and Krypton

For examination of $\eta\rho T$ results obtained with the advanced viscometer-densimeter, viscosity measurements on nitrogen, argon, and helium were carried out with the new apparatus on the 293.15 K isotherm. Moreover, viscosity measurements on krypton were carried out at 298.15 K. The measurements took place at low pressures, and the densities were calculated from equations of state, namely the reference equation of state for nitrogen of Span et al. [43], the reference equation of state for argon of Tegeler et al. [44], the equation of state for helium of McCarty and Arp [45], and the equation of state for krypton of Juza and Šifner [46]. The substances were identical with those investigated with the combined viscometer-densimeter (see Section 4).

As an example, the $\eta\rho T$ data of helium measured with the new apparatus are compared with the measurements of the combined viscometer-densimeter and with selected results of other authors in Fig. 10. The diagram shows deviations of the data relative to a simple regression function that was fitted to the data of the combined viscometer-densimeter. The uncertainty of the data of the special apparatus is illustrated as a shaded

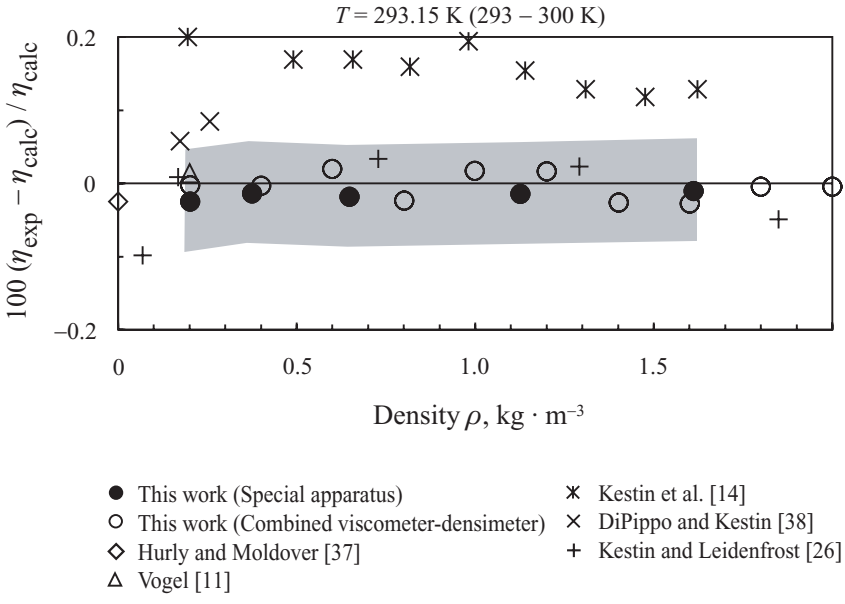

Fig. 10. Measurements of viscosity data of helium with the special apparatus for low densities in comparison with the experimental viscosities of the advanced combined viscometer-densimeter and of other authors. The zero line is calculated from a regression function based on the data of the combined viscometer-densimeter. The shaded area corresponds to the experimental uncertainty of the measurements with the special apparatus for low densities in this work.

area. The data of the special apparatus confirm the results of the combined viscometer-densimeter with deviations within $\pm 0.03\%$, which corresponds to the scatter of the data of the combined viscometer-densimeter. Excellent agreement within the uncertainty of the data of the special apparatus is also observed with the results of Hurly and Moldover [37], Vogel [11], and Kestin and Leidenfrost [26]. The data sets of these authors can be considered as very accurate in the low density area. The data of DiPippo and Kestin [38] differ by about $+0.1\%$ from the new data, and the data set of Kestin et al. [14] shows a systematic deviation of less than $\pm 0.2\%$.

6. CONCLUSION

An apparatus for the simultaneous measurement of viscosity and density of fluids has been presented. The viscometer-densimeter covers a viscosity range up to 150 μPa·s and a density range up to 2000 $kg \cdot m^{-3}$ at temperatures from 233 to 523 K and pressures up to 30 MPa. The apparatus

achieves uncertainties of ± 0.02 to $\pm 0.05\%$ in density and uncertainties in viscosity of less than ± 0.15 to $\pm 0.4\%$. The measuring principles are absolute. Therefore, the apparatus can be used as a primary standard.

Comprehensive $\eta\rho T$ measurements were carried out on nitrogen, argon, and methane over the entire working range of the viscometer-densimeter. In addition, $\eta\rho T$ measurements on helium, neon, and krypton were made on two selected isotherms each. The remarkable consistency of the data sets and the comparison with the experimental results of other authors show that the estimated total uncertainties mentioned above are clearly met.

Moreover, a special instrument for very accurate viscosity measurements at low densities has been designed. The estimated uncertainty of this viscometer is less than $\pm 0.07\%$. Viscosity measurements on nitrogen, helium, argon, and krypton carried out with this apparatus confirmed the data of the combined viscometer-densimeter within $\pm 0.03\%$.

The combined viscometer-densimeter and the new special viscosity apparatus represent outstanding advances to the field of thermophysical research. Both are capable of serving as primary standards in viscosity.

ACKNOWLEDGMENTS

The authors are grateful to all who contributed to this work. Above all, we thank the Deutsche Forschungsgemeinschaft for the financial support of this project.

REFERENCES

1. A. H. Krall, J. C. Nieuwoudt, J. V. Sengers, and J. Kestin, *Fluid Phase Equil.* **36**:207 (1987).
2. A. A. H. Padua, J. M. N. A. Fareleira, J. C. G. Calado, and W. A. Wakeham, *Int. J. Thermophys.* **17**:781 (1998).
3. F. Audonnet and A. A. H. Padua, *Fluid Phase Equil.* **181**:147 (2001).
4. A. Docter, H. W. Lösch, and W. Wagner, *Fortschr.-Ber. VDI-Z., Ser.*3, No. 494 (1997).
5. A. Docter, H. W. Lösch, and W. Wagner, *Int. J. Thermophys.* **20**:485 (1999).
6. H. W. Lösch, R. Kleinrahm, and W. Wagner, in *Jahrbuch 1994 "Verfahrenstechnik und Chemieingenieurwesen"*, VDI Gesellschaft Verfahrenstechnik und Chemieingenieurwesen (VDI-Verlag, Düsseldorf, 1994), pp. 117–137.
7. W. Wagner, K. Brachthäuser, R. Kleinrahm, and H. W. Lösch, *Int. J. Thermophys.* **16**:399 (1995).
8. W. Wagner, R. Kleinrahm, H. W. Lösch, and R. T. Watson, in *IUPAC Experimental Thermodynamic, Vol. VI: Measurements of the Thermodynamic Properties of Single Phases*, A. R. H. Goodwin, K. N. Marsh, and W. A. Wakeham, eds. (Elsevier, Amsterdam, 2002), in press.

9. V. Vasanta Ram, *Eine Lösung der zeitabhängigen Navier–Stokes-Gleichungen für ein konzentrisches Zylindersystem* (Arbeitsbericht des Lehrstuhls für Strömungsmechanik, Ruhr-Universität Bochum, 1996).
10. K. Stephan, R. Krauss, and A. Laesecke, *J. Phys. Chem. Ref. Data* **16**:993 (1987).
11. E. Vogel, *Ber. Bunsenges. Phys. Chem.* **88**:997 (1984).
12. A. G. Clarke and E. B. Smith, *J. Chem. Phys.* **51**:4156 (1969).
13. J. Kestin, S. T. Ro, and W. A. Wakeham, *Ber. Bunsenges. Phys. Chem.* **86**:753 (1982).
14. J. Kestin, E. Paykoc, and J. V. Sengers, *Physica* **54**:1 (1971).
15. J. H. B. Hoogland, H. R. van den Berg, and N. J. Trappeniers, *Physica* **134A**:169 (1985).
16. J. A. Gracki, G. P. Flynn, and J. Ross, *J. Chem. Phys.* **51**:3856 (1969).
17. G. P. Flynn, R. V. Hanks, N. A. Lemaire, and J. Ross, *J. Chem. Phys.* **38**:154 (1963).
18. A. Michels and R. O. Gibson, *Proc. Roy. Soc.* **A134**:288 (1931).
19. B. Latto and M. W. Saunders, *Can. J. Chem. Eng.* **50**:765 (1972).
20. D. E. Diller, *Physica* **119A**:92 (1983).
21. B. A. Younglove and H. J. M. Hanley, *J. Phys. Chem. Ref. Data* **15**:1323 (1986).
22. G. C. Maitland and B. E. Smith, *J. Chem. Eng. Data* **17**:150 (1972).
23. J. Kestin, S. T. Ro, and W. A. Wakeham, *J. Chem. Phys.* **56**:4119 (1972).
24. R. A. Dawe and E. B. Smith, *J. Chem. Phys.* **52**:693 (1970).
25. A. G. Clarke and E. B. Smith, *J. Chem. Phys.* **48**:3988 (1968).
26. J. Kestin and W. Leidenfrost, *Physica* **25**:1033 (1959).
27. J. Wilhelm and E. Vogel, *Int. J. Thermophys.* **21**:301 (2000).
28. A. Michels, A. Botzen, and W. Schuurmann, *Physica* **20**:1141 (1954).
29. W. M. Haynes, *Physica* **67**:440 (1973).
30. J. Kestin and J. W. Whitelaw, *Physica* **29**:335 (1963).
31. D. G. Friend, J. F. Ely, and H. Ingham, *J. Phys. Chem. Ref. Data* **18**:583 (1989).
32. Y. Abe, J. Kestin, H. E. Khalifa, and W. A. Wakeham, *Physica* **93A**:155 (1978).
33. J. Kestin and S. T. Ro, *Ber. Bunsenges. Phys. Chem.* **80**:619 (1976).
34. D. E. Diller, *Physica* **104A**:417 (1980).
35. J. G. Giddings, T. F. Kao, and R. Kobayashi, *J. Chem. Phys.* **45**:578 (1966).
36. L. T. Carmichael, V. Berry, and B. H. Sage, *J. Chem. Eng. Data* **10**:57 (1965).
37. J. J. Hurly and M. R. Moldover, *J. Res. Nat. Inst. Stand. Tech.* **105**:667 (2000).
38. R. DiPippo and J. Kestin, *Proc. Fourth Symp. Thermophys. Props.* (ASME, New York, 1968), p. 304.
39. V. A. Rabinovich, A. A. Vassermann, V. I. Nedostup, and L. S. Veksler, *Thermophysical Properties of Neon, Argon, Krypton, and Xenon*, National Standard Reference Data Service of the USSR (Hemisphere Publishing, New York, 1988).
40. J. Kestin and A. Nagashima, *J. Chem. Phys.* **40**:3648 (1964).
41. H. R. van den Berg, *Precisiemetingen aan de Viscositeitscoefficient van Krypton en de logarithmische Term in de Dichtheidsontwikkeling*. Dissertation (Universiteit van Amsterdam, 1979).
42. N. J. Trappeniers, A. Botzen, J. van Ooosten, and H. R. van den Berg, *Physica* **31**:945 (1965).
43. R. Span, E. W. Lemmon, R. T. Jacobsen, W. Wagner, and A. Yokozeki, *J. Phys. Chem. Ref. Data* **29**:1361 (2000).
44. C. Tegeler, R. Span, and W. Wagner, *J. Phys. Chem. Ref. Data* **28**:779 (1999).
45. R. D. McCarty and V. D. Arp, *Adv. Cryog. Eng.* **35**:1465 (1990).
46. J. Juza and O. Šifner, *Acta Tech. CSAV* **1**:1 (1986).